# Dystroglycan is involved in skin morphogenesis downstream of the Notch signaling pathway

Cathy Sirour[a], Magdalena Hidalgo[a,b], Valérie Bello[a], Nicolas Buisson[a], Thierry Darribère[a], and Nicole Moreau[a]

[a]Laboratoire de Biologie du Développement, Université Pierre et Marie Curie, Sorbonne Universités, UMR CNRS 7622, 75252 Paris Cedex 05, France; [b]Laboratoire Réponses Cellulaires et Fonctionnelles à l'Hypoxie, Université Paris13, EA2363, 93017 Bobigny Cedex, France

**ABSTRACT** **Dystroglycan (Dg) is a transmembrane protein involved both in the assembly and maintenance of basement membrane structures essential for tissue morphogenesis, and the transmission of signals across the plasma membrane. We used a morpholino knockdown approach to investigate the function of Dg during *Xenopus laevis* skin morphogenesis. The loss of Dg disrupts epidermal differentiation by affecting the intercalation of multiciliated cells, deposition of laminin, and organization of fibronectin in the extracellular matrix (ECM). Depletion of Dg also affects cell–cell adhesion, as shown by the reduction of E-cadherin expression at the intercellular contacts, without affecting the distribution of $\beta_1$ integrins. This was associated with a decrease of cell proliferation, a disruption of multiciliated-cell intercalation, and the down-regulation of the transcription factor P63, a marker of differentiated epidermis. In addition, we demonstrated that inhibition or activation of the Notch pathway prevents and promotes transcription of *X-dg*. Our study showed for the first time in vivo that Dg, in addition to organizing laminin in the ECM, also acts as a key signaling component in the Notch pathway.**

**Monitoring Editor**
Marianne Bronner-Fraser
California Institute of Technology

Received: Jan 28, 2011
Revised: May 18, 2011
Accepted: Jun 9, 2011

## INTRODUCTION

During embryogenesis, the extracellular matrix (ECM) composition and organization is strictly regulated and modified to modulate tissue morphogenesis and organogenesis (Tsang *et al.*, 2010). The ECM provides both signals and mechanical support to integrate cells in a tissue (Bateman *et al.*, 2009). Abnormal organization or composition of the ECM often leads to developmental defects and/or lethality (Tsang *et al.*, 2010).

Basement membranes (BMs) are specialized components of the ECM that provide tissue structure and influence cell behavior. They are composed, in part, of a characteristic set of large extracellular glycoproteins (laminins, entactin, nidogen, and type IV collagen), but individual BMs differ in their composition, leading to an abundance of diverse interacting partners and added complexity (Van Agtmael and Bruckner-Tuderman, 2010). Laminin is, besides collagen, the most abundant BM component and is present in all BM.

Although the most intensively studied receptors for laminins are integrins, another essential laminin receptor, dystroglycan (Dg), forms a large complex containing a spectrin-like actin-binding protein (Winder, 1997). The Dg complex was originally identified in studies on muscular dystrophy (Ervasti and Campbell, 1991) and subsequently shown to play important roles in the cell–ECM interactions in both muscle and epithelial cells (Barresi and Campbell, 2006).

Dg is composed of two noncovalently associated subunits, namely an extracellular α-Dg and a transmembrane β-Dg, that are posttranslationally cleaved from a single precursor protein (Barresi and Campbell, 2006). α-Dg is heavily glycosylated with a unique *O*-mannosyl oligosaccharide and is responsible for laminin binding, while the cytoplasmic tail of β-Dg binds to utrophin or dystrophin, the spectrin-like molecules that interact with a number of proteins, including F-actin (Winder, 1997). Most of the regulatory controls on Dg expression are exerted posttranslationally (Bozzi *et al.*, 2009). No

This article was published online ahead of print in MBoC in Press (http://www.molbiolcell.org/cgi/doi/10.1091/mbc.E11-01-0074) on June 16, 2011.

Address correspondence to: Nicole Moreau (nicole.moreau@upmc.fr).

Abbreviations used: ALP, alkaline phosphatase; BM, basement membrane; CCP, ciliated cell precursor; CMo, mismatch Dg morpholino oligonucleotide; Dg, dystroglycan; DgMo, *dg* antisense morpholino; ECM, extracellular matrix; EGTA, ethyleneglycoltetraacetic acid; FITC, fluorescein isothiocyanate; INC, intercalating nonciliated cell; PMSF, phenylmethylsulfonyl fluoride; qRT-PCR, quantitative real-time PCR; SEM, scanning electron microscopy.

molecular details underlying transcriptional regulation are currently available. Dg is essential for BM formation in several tissues, including epithelia, and is involved in epithelial cell polarity (Durbeej *et al.*, 1995; Michele *et al.*, 2002; Masuda-Hirata *et al.*, 2009). Dg-null mice die early in embryogenesis due to a failure of extraembryonic BM formation (Williamson *et al.*, 1997). Conditional ablation of the Dg gene in mammary epithelial cells abolishes laminin binding to the cell surface and disrupts cellular polarity (Weir *et al.*, 2006).

In *Xenopus* embryos, localized expression of *Dg* transcripts (*X-dg*) was first detected at the end of gastrulation (Moreau *et al.*, 2003). At this stage, *X-dg* is essentially confined to the notochord and subsequently found at the level of the somite. This expression is concomitant with the appearance of laminin in the ECM of these tissues (Fey and Hausen, 1990). Depletion of Dg leads to defect in laminin deposition at the intersomitic junction (Hidalgo *et al.*, 2009). Dg is also crucial for laminin assembly in ECM, and provides a signaling cascade regulating cell proliferation of pronephros epithelial cells (Bello *et al.*, 2008). Cells expressing *X-dg* are also detected in the neural plate and epidermal ectoderm at stage 15. This expression is limited to the sensorial layer of the epidermis at stage 22 (Lunardi and Dente, 2002; Moreau *et al.*, 2003).

In *Xenopus*, the embryonic ectoderm is fated to become either neural or nonneural epidermis due to patterning processes occurring before and during gastrulation (Wilson and Hemmati-Brivanlou, 1995). The skin develops after gastrulation through the differentiation of two cell types derived from two distinct layers of the epidermal ectoderm (Drysdale and Elinson, 1992). Cells in the outer layer of the ectoderm, also called the superficial layer, differentiate into mucus-producing epidermal cells. Cells in the inner layer of the ectoderm, also called the sensorial layer, spread out underneath the outer layer during epiboly (Keller, 1980). In the inner layer, a subset specified by the Notch pathway gives rise during early neurulation to ciliated cells precursors (CCPs), which express the α-tubulin gene, and intercalating nonciliated cells (INCs; Drysdale and Elinson, 1992; Deblandre *et al.*, 1999; Stubbs *et al.*, 2006). These two cell types then intercalate radially into the outer layer at midneurulation. The ciliated cells cover the skin in a characteristic spacing pattern that results from the intercalation process. After neurulation, cells of the sensorial layer flatten and express a specific transcription factor named P63 (Lu *et al.*, 2001). P63 is related to the tumor suppressor and transcription factor P53 (Levrero *et al.*, 2000; Yang and McKeon, 2000). Mice lacking the P63 gene have severe developmental defects. They lack all squamous epithelia and their derivatives; such mice die shortly after birth due to dehydration (Mills *et al.*, 1999; Yang *et al.*, 1999). In zebrafish, the orthologous DeltaNP63 acts as a transcriptional repressor required for ventral specification of the ectoderm during gastrulation. It is described as an ectoderm-specific direct transcriptional target of BMP signaling. Loss of DeltaNp63 function leads to reduced nonneural ectoderm, followed by defects in epidermal development during skin and fin bud formation (Bakkers *et al.*, 2002).

We show that *X-dg* mRNA is present in nonexpressing *α-tubulin* cells in the sensorial layer of the *Xenopus* epidermis as early as midneurulation. Loss of Dg function produces numerous disorders during skin differentiation, both at the morphological and molecular levels. At the morphological level, we observe a diminution of cell–cell contacts, a disruption of CCPs intercalation, and the absence of flattening of the inner-layer cells. At the molecular level, a loss of Dg function abolishes deposition of laminin in the epidermal ECM and reduces E-cadherin expression at the intercellular contacts and maintenance of fibronectin matrix. We demonstrate that the expression of P63 is lost, and cell proliferation is reduced. We also demonstrate that the Notch pathway up-regulates *X-dg* transcription. Finally, the results show an epistatic relationship among Notch, Dg, and P63 in control of skin morphogenesis.

## RESULTS

### Expression of *X-dg* during epidermal ectoderm differentiation

We previously described the expression pattern of *X-dg* transcripts in *Xenopus laevis* during development (Moreau *et al.*, 2003). Using an *X-dg* antisense RNA probe, we detected the transcripts in a variety of tissues and cell types. In this paper, we focus the analysis on *X-dg* expression in the epidermal ectoderm during the course of its differentiation.

We examined the expression pattern using whole-mount, in situ hybridization and subsequent sections (Figure 1). In epidermal ectoderm, the *X-dg* signal appeared at stage 14/15 in the posterior

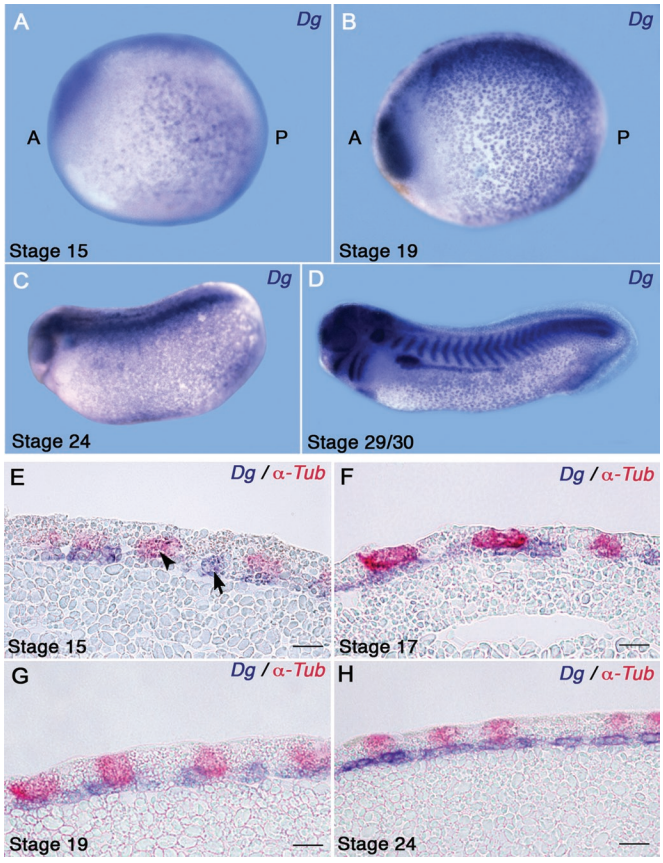


FIGURE 1: *Dystroglycan* and *α-tubulin* expression during epidermal ectoderm differentiation. (A–D) Whole-mount, in situ hybridizations were performed using the *X-dg* probe at stage 15 (A), stage 19 (B), stage 24 (C), and stage 29/30 (D). Lateral views show that Dg transcripts are present in a regularly spaced pattern at the embryonic surface. They are also present in brain, optic and otic vesicles, visceral arches, somites, pronephros, and pronephric duct. (E–H) Embryos were double-labeled by whole-mount, in situ hybridization for *X-dg* (blue-purple) and *α-tubulin* (red) transcripts, and then cryostat-sectioned. Stage 15 (E), stage 17 (F), stage 19 (G), and stage 24 (H). In (E) there is no overlapping of the two gene expression domains in the sensorial layer. Arrowhead: cell expressing *α-tubulin* transcripts, arrow: cell expressing *X-dg* transcripts. When CCPs (red) intercalate, they are devoid of *X-dg* (F–H); the *X-dg* expression becomes stronger in sensorial layer and cells progressively flattened. A: anterior; P: posterior. Scale bars: 10 μm.

region of the embryo (Figure 1A) and progressed to the anterior region up to stage 19 (Figure 1B). The expression was scattered from stage 15 to stage 19, then it spread out, as observed at stage 24 (Figure 1C). The signal was still observed at stage 29/30 (Figure 1D).

### Dg is not expressed by CCPs

During neurulation (stages14–19), a subset of the epidermal sensorial layer gives rise to CCPs, which express α-*tubulin* and differentiate by intercalating radially into the outer layer (see *Introduction*). Since α-*tubulin* and *X-dg* are simultaneously expressed in the sensorial layer, we were interested by their relative pattern of expression in this layer. To specify the spatiotemporal expression of *X-dg* versus α-*tubulin*, we used double whole mount in situ hybridization and subsequent histological sections using *X-dg* and α-*tubulin* cRNA probes.

At stage 15, we observed expression of the two genes without any overlapping of the two expression domains (Figure 1E). From late stage 15 and onward, the CCPs began to intercalate radially into the superficial layer, while the *X-dg* expression became stronger in the sensorial layer (Figure 1, F–H). At stage 19, all the CCPs reached the superficial layer, and the *X-dg*–expressing cells were now adjacent in the inner layer of the ectoderm (Figure 1G). The inner cells continued to express *X-dg* and progressively flattened and spread out underneath the outer layer, while the multiciliated cells reached their fully differentiated state (stage 24, Figure 1H). It appeared that, in the sensorial layer, cells that expressed α-*tubulin* did not express *X-dg*. The two cell types were distributed in an evenly spaced pattern, suggesting a lateral inhibition mechanism of regulation.

### Dg depletion disrupts epidermal ectoderm differentiation

We knocked down *X-dg* by using two *dg* antisense morpholinos (DgMo). Their specificity and efficiency were demonstrated previously (Bello *et al.*, 2008; Hidalgo *et al.*, 2009). Injections with 16 ng of morpholinos in each cell were performed in both left blastomeres at the four-cell stage. We previously described this amount leading to a significant reduction of Dg protein, which did not induce too drastic morphological abnormalities in the embryos (Bello *et al.*, 2008). The uninjected half of each embryo represents the internal control of the experiment. The toxicity of morpholinos and specificity of phenotypes observed were controlled in the same conditions by injection of a mismatch *dg* morpholino oligonucleotide (CMo).

The surfaces of the embryos were studied by scanning electron microscopy (SEM) during differentiation of epidermal ectoderm. Observations were performed on stage 13 embryos, as this stage corresponds to the beginning of epidermal morphological differentiation (Billett and Gould, 1971), and on stage 28 embryos, as the epidermis is fully differentiated in this stage. We focused our observations to the lateral trunk epidermis, since ciliated cell distribution in differentiated epidermis varies with body region (Nokhbatolfoghahai *et al.*, 2005). There was no difference between the epidermis of CMo-injected and uninjected embryos, so we selected photographs from CMo-injected embryos for all the figures. At stage 13, the epidermal surface of the CMo- or DgMo-injected sides of embryos were composed of polygonal cells with prominent and lineal intercellular limits. The size of these cells was nearly identical (Figure 2, A and D). The outer ectodermal surface is devoid as in regular development of multiciliated cells at this stage.

At stage 28, the epidermal surface of the CMo-injected sides of embryos were composed of a heterogeneous mosaic of regular polygonal cells. The ciliated cells (identified by large clusters of cilia emerging from their apical surfaces) were interspaced regularly between nonciliated cells. The nonciliated cells were mainly secreting cells. Distinct straight lineal and prominent boundaries were evident between the cells (Figure 2B). Ciliated cells made contact with four or five of the large secreting cells. This arrangement represents a specific pattern similar to the corolla of flowers; the multiciliated cell occupies the central area of the corolla (Figure 2C). The epidermal surfaces of the DgMo-injected sides of embryos were composed of cells arranged in irregular polygonal patterns. Their boundaries appeared flattened. The surfaces of large secreting cells were greater than in controls (Figure 2E), suggesting cell proliferation was reduced. This reduction of proliferation was confirmed by using an anti-phosphohistone H3 antibody as a mitosis marker. At stage 24, the proliferation was reduced by 35% in epidermis of DgMo-injected sides of the embryos ($n = 20$; the positive cells were counted on the same surface area of the lateral trunk epidermis [Supplemental Figure S1]). The number of ciliated cells was reduced, and they were irregularly scattered and often positioned side by side, a pattern that was never observed in controls. The typical corolla of flowers pattern disappeared (Figure 2F). To quantify the decreasing number of ciliated cells, indirect immunofluorescence using an antibody to acetylated α-tubulin was performed (Figure 2G). At stage 28, the quantification (in the same surface area of the lateral trunk epidermis) on both DgMo-injected and noninjected sides of the embryos ($n = 10$) showed a 30% reduction of differentiated ciliated cells in the injected side (Figure 2H). To analyze the organization of cells in the two ectodermal layers, ultrathin sections were performed. The control showed two layers of cuboidal cells at stage 13; the outer-layer cells were tightly cohesive, unlike the inner-layer cells (Figure 2I). At stage 24, in the inner layer, cells were flat and closely associated (Figure 2J). At stage 13, the epidermal layers of the DgMo-injected sides were nearly similar to the control sides (Figure 2K). At stage 24, the cells of the superficial layers were greater, and numerous cells were interspaced between the outer and inner layers. The inner cells as the outer cells were greater; in addition, they were loosely associated, extended numerous filopodia, and did not flatten (Figure 2L). Among the cells interspaced between the outer and inner layers, we identified (by double in situ hybridization with *X-dg* and α-*tubulin*) ciliated cell precursors that were not able to reach the outer layer. We never observed *X-dg*–expressing cells among the interspaced cells (Figure 2, M and N), suggesting that, without Dg, there are failures in the radial intercalation processes.

The previous results demonstrate that the structure of the epidermis is affected by the loss of Dg, essentially at the level of cell proliferation, distribution of multiciliated cells, and cell adhesion.

### Dg is critical for the intercalation of the precursors of ciliated cells

Dg is expressed only in the sensorial layer, but the reduction of Dg affects the structure and organization of the two layers of the epidermis, and especially the number of ciliated cells of the outer layer. This suggests that Dg acts in a non-cell-autonomous manner. To analyze Dg function, we grafted the outer-layer ectoderm from a control embryo onto the inner layer of an injected host embryo at the beginning of gastrulation. The explant corresponds to the prospective region of epidermal ectoderm, and the graft was done in the same region, namely the ventral ectoderm (Figure 3A). The donor cells were labeled by the injection of RNA encoding membrane-localized forms of green fluorescent protein (GFP; GFP-ras mRNA) in the four animal blastomeres at the eight-cell stage. The host embryo was injected in the same conditions with DgMo or CMo. At stage 28, when the larval skin was fully differentiated, the epidermis

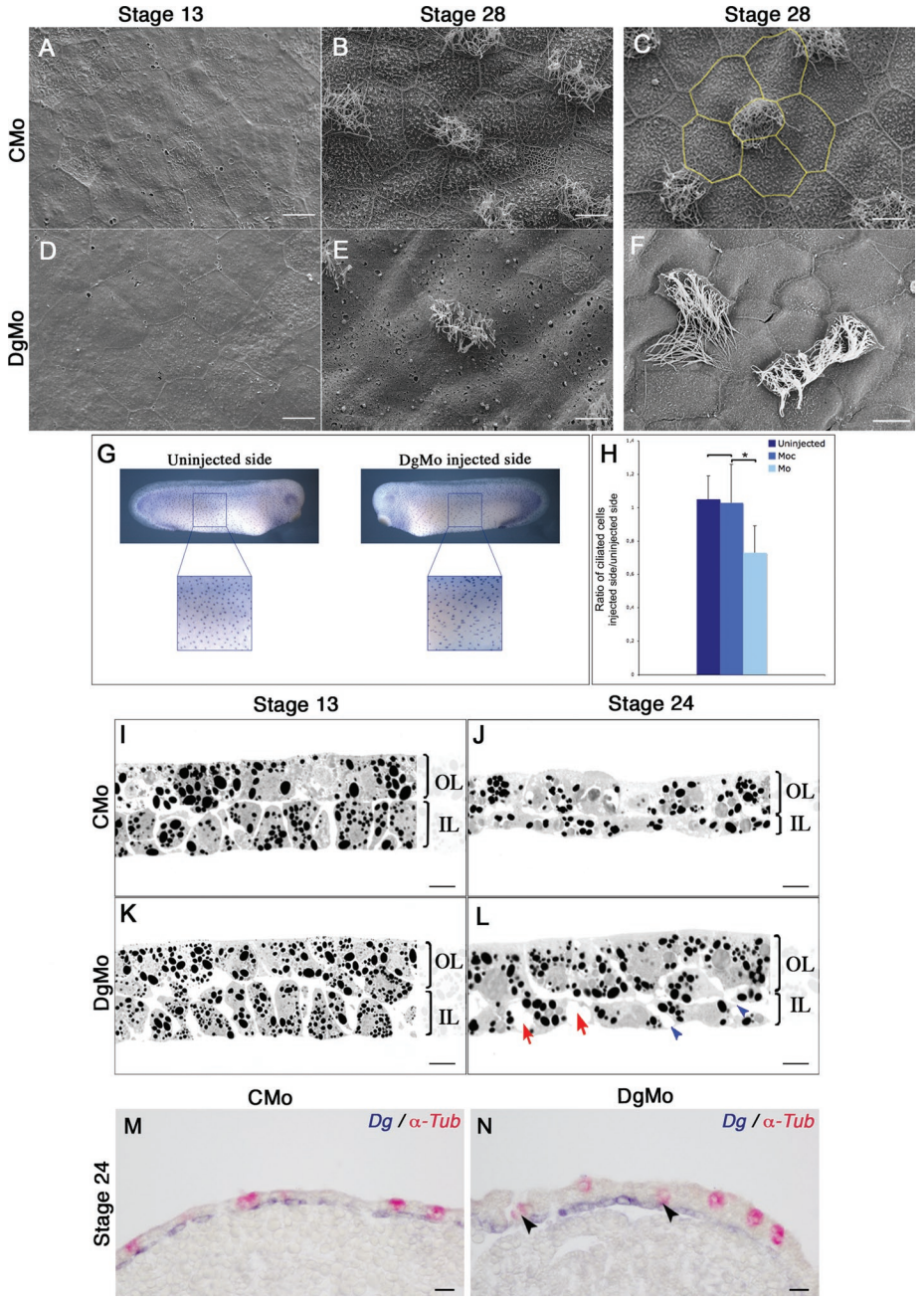


FIGURE 2: Dg depletion disrupts epidermal ectoderm differentiation. (A–F) SEM of skin embryo at stages 13 (A and D) and 28 (B, C, E, and F). At stage 13, the epidermal surface is identical in CMo and DgMo embryos (A and D). The outer ectodermal surface is devoid of ciliated cells. At stage 28, Dg depletion causes a decrease of the number of ciliated cells, a lack of linear aggregates, and a flattening of the cell–cell boundaries (compare B and E). The yellow feature underlines the flower corolla pattern of the outer cell layer (C). Ciliated cells are often positioned side by side in the Dg depletion context and the specific pattern disappears (F). (G–H) Whole-mount immunostaining of α-tubulin with 6-11B-1 antibodies: the DgMo-injected side presents a decrease of the number of ciliated cells (G). Ratio analysis of the number of ciliated cells of the injected side/uninjected side, which shows a decrease of 30% in the Dg depletion context (n = 10). *, Statistically significant difference (*t* test: p = 0.007; H). (I–L) Thin sections of skin at stages 13 (I and K) and 28 (J and L). At stage 13, sections of the uninjected embryo show a double layer of cuboidal cells (I), the epidermis of the DgMo embryo is nearly similar to the control (K). In control at stage 28, when the skin has fully differentiated, the outer layer contains large, tightly adhered columnar cells. The inner layer exhibits smaller, flattened, and adherent cells (J). The epidermis of the injected embryo shows a thickening of the skin and a less cohesive tissue. In particular, inner cells do not spread and do not flatten; they are loosely associated. The intercellular spaces (red arrows) are enlarged. Numerous cytoplasmic protrusions extend from cell to cell (blue arrowheads; L). IL: inner layer; OL: outer layer. (M–N) Embryos were injected with CMo or DgMo and fixed at stage 24. Double whole-mount, in situ hybridization for *X-dg* (blue-purple) and *α-tubulin* (red) transcripts was performed; embryos were then cryostat-sectioned. In the control, all CCPs have reached the outer layer (M), whereas in embryos injected with Mo, some CCPs are trapped between the two layers (N, black arrowheads). Scale bars: 10 μm.

in the graft region was excised. In this tissue, the superficial cells coming from the donor expressed GFP at cell–cell contacts. The apical junctions were marked with antibodies to ZO-1. The cells of the sensorial layer coming from the host by radial intercalation were GFP-negative. The ciliated cells were identified by indirect immunofluorescence using acetylated α-tubulin antibody. The surface layer cells were sliced from apical to basal surface using confocal microscopy (Figure 3). The number of acetylated α-tubulin-positive cells/total cell number in the same surface area was identical in control and DgMo embryos (n = 8), suggesting Dg does not regulate the Notch lateral inhibition process. In hosts injected with CMo, the ciliated cells were GFP-negative, regularly interspaced, and in contact with four to five large GFP-positive cells. The GFP cells were polygonal; their basal and apical surfaces were identical in size (Figure 3, B and B′). Small, GFP-negative cells corresponding to nonciliated cells were also interspaced in this layer. The apical membranes were continuously labeled with ZO-1 antibodies. The apical and basal contacts between cells were narrow. We never observed the juxtaposition of two ciliated cells. The ciliated cells extended from the apical to the basal region of the surface layer, with a basal surface larger than the apical one (Figure 3, B and B′). These results suggest that all host CCPs have achieved their radial intercalation and are fully differentiated at stage 28 (Figure 3D). In host embryos injected with DgMo, the apical domain of all cells was larger than in controls, and the tight contacts were not affected. In contrast, the basal surface of the cells was irregular, with fewer intercellular contacts, suggesting defects in cell–cell adhesion. Both the ciliated cells and the small GFP-negative cells were irregularly interspaced. Among the acetylated α-tubulin-positive cells, some extended from the apical to basal domain of the tissue as in the control, but others were trapped below the surface (Figure 3, C, C′, and E), suggesting that their radial intercalation was incomplete (Figure 3, E and F). These results show that Dg is required for

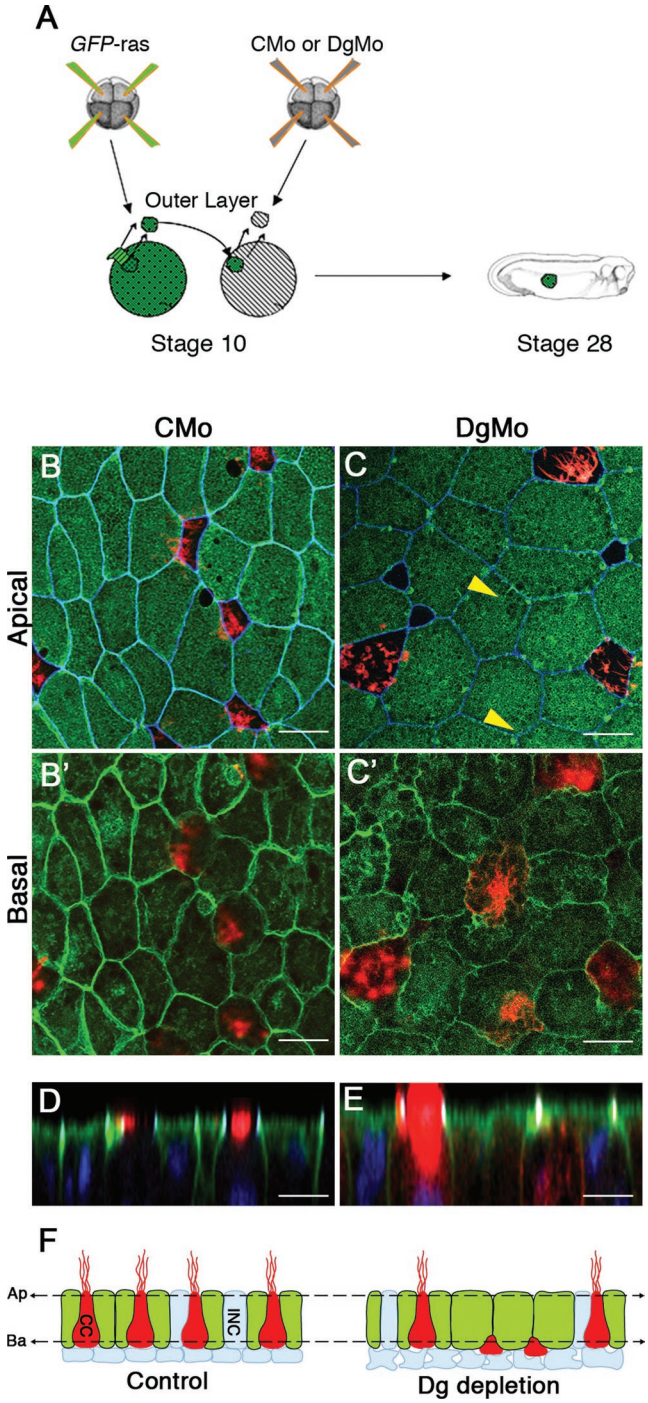


FIGURE 3: Dg depletion impairs the radial intercalation of ciliated cells. (A) Schematic drawing of the experimental procedure. Transplants were excised on early-gastrula-stage embryos. An outer layer from a *GFP-ras* mRNA-injected embryo was grafted on the inner layer of a DgMo- or CMo-injected embryo. Embryos were allowed to develop until stage 28. (B–C′) A triple indirect immunofluorescence was performed to detect ZO-1 (blue), GFP (green), and α-tubulin (red). (B and C) Confocal slices through the apical surface of the outer layer. (B′ and C′) Confocal slices within 8 µm of the apical surface within the same field. All cells labeled by α-tubulin antibodies in the basal side are labeled in the apical side in CMo (B and B′) conditions. In the Mo context (C and C′), some cells labeled basally do not appear apically (yellow arrowhead). (D–E) Transverse (*z*-axis) confocal reconstruction (nuclei: blue; GFP: green; α-tubulin: red). An α-tubulin-labeled cell extended from the apical to basal domain; another was trapped below the surface (yellow arrowhead). (F) Schematic drawing representing the radial intercalation of ciliated cells in a control and in a Dg depletion context (modified from Stubbs *et al.*, 2006). CC: ciliated cell; INC: intercalating nonciliated cell; Ap: apical; Ba: basal. Scale bars: 10 µm.

CCP intercalation and maintenance of lateral cell–cell contacts in the epidermal outer layer.

Given the defects observed in cell adhesion, and the essential role of cell adhesion and ECM molecules in intercalation, we then investigated the expression of E-cadherin, fibronectin, and laminin in embryos with reduced Dg expression.

### Dg depletion inhibits laminin-1 deposition and disorganizes fibronectin meshwork in ECM

To investigate the effect of Dg depletion to ECM assembly, embryos were injected unilaterally at the four-cell stage with CMo or DgMo and GFP-ras mRNA to delineate cell borders. At stage 19, the lateral trunk ectoderm was peeled off and then labeled with anti-laminin or anti-fibronectin antibodies. The inner side of the ectoderm was observed by confocal microscopy (Figure 4A). In control explants, the inner ectodermal cells were polygonal; their GFP tagged membranes appeared cohesive. Fibronectin was assembled into fibrillar structures and formed an extensive meshwork across the cell surface (Figure 4, B and C). Laminin appeared assembled into short fibrils across the cell surface (Figure 4D). In the control the membrane staining appears tight and relatively linear, while in DgMo it is wider with apparent gaps, suggesting defects in cell adhesion. Consequently the intercellular space was enlarged (Figure 4E). The fibronectin fibrils localized on cell surface, but not across the intercellular space (Figure 4F). In contrast to fibronectin, the ECM was completely devoid of laminin (Figure 4G).

### Dg depletion reduces E-cadherin expression at the cell–cell contacts, but $\beta_1$ integrin is not affected

As the intercellular adhesions are affected when Dg is knockdown, we wondered whether the expression of E-cadherin and $\beta_1$ integrin might be affected in Dg-Mo embryos. Indirect immunofluorescence, performed at stage 19, revealed a weaker expression of E-cadherin at the level of cell–cell contacts in the two epidermal layers of Dg-Mo embryos when compared with controls (unpublished data). These differences were amplified at stage 24, where the immunoreactivity for E-cadherin was almost undetectable at the cell membranes (Figure 4, H, I, and L). In contrast, $\beta_1$-integrin distribution was never affected (Figure 4, J, K, and L). Four independent Western blot analyses of Mo-injected tissues from stage-24 embryos using anti-Dg, anti–E-cadherin, and anti–$\beta_1$-integrin antibodies were performed. No significant variation of E-cadherin and $\beta_1$ integrin was detected, but Dg was absent in the Mo-injected epidermis (Figure 4M). To test whether the reduction in E-cadherin expression at the cell membranes was due to perturbation of *E-cadherin* transcription, we quantified the gene expression level of E-cadherin in Mo-injected embryos. Surprisingly quantitative real-time PCR (qRT-PCR) analysis normalized to ornithine decarboxylase, showed a significant up-regulation of E-cadherin expression (Figure 4N).

These results show that Dg controls laminin deposition and E-cadherin localization to the cell membrane, but it does not perturb the expression of E-cadherin mRNA and protein. Further studies will address whether E-cadherin mislocalization is a direct consequence of the loss of Dg and/or an indirect consequence of the absence of laminin.

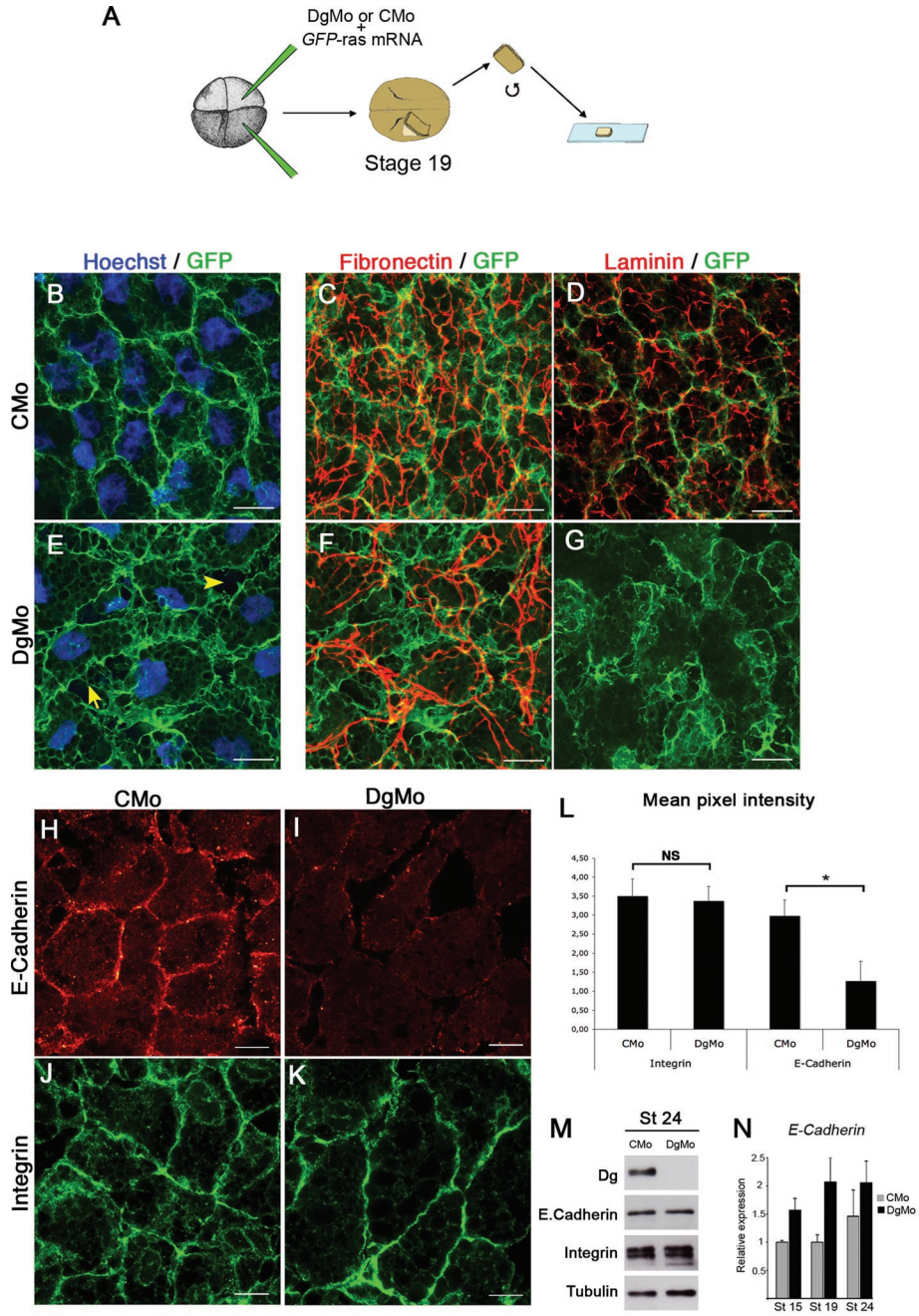


FIGURE 4: Dg depletion inhibits laminin-1 deposition and disorganizes fibronectin meshwork in ECM. It reduces E-cadherin expression at the cell–cell contacts, while $\beta_1$ integrin is not affected. (A) Schematic drawing of the experimental procedure. Four-cell-stage embryos were unilaterally injected with CMo or DgMo + *GFP-ras* mRNA to delineate cell borders, allowed to develop until stage 19 or 24, and then fixed. A piece of epidermis was peeled off. (B–G) Whole mount at stage 19 of the basal face of the epidermis was observed by confocal microscopy. Nuclei were labeled with Hoechst (blue), the cell membrane appears in green (*GFP-ras* mRNA), and fibronectin or laminin were detected by indirect immunofluorescence (red). In CMo, the green fluorescence finely delineates the cell–cell contacts (B), while it appears diffuse in DgMo, suggesting cell–cell cohesion is affected by the Dg depletion. The cells still exhibit important intercellular spaces (arrowhead) and numerous highly formed filopodia radiate all around the cells (arrow; E). In DgMo, indirect immunofluorescence shows a disorganization of the fibronectin network (F) and the absence of laminin in the ECM (G), as compared with CMo (C and D). (H–K) Immunostaining of E-cadherin and $\beta_1$ integrin at stage 24. Confocal imaging was done on the inner cells of epidermis pieces. The expression of E-cadherin was weaker in embryos injected with DgMo (I) than with CMo (H). (J and K) $\beta_1$-integrin expression was not affected. (L) Mean E-cadherin and β1-integrin pixel intensity (see *Materials and Methods* for details) in CMo and DgMo. *, Statistically significant difference (*t* test: $p = 0.045$). (M) Western blot analysis of Mo-injected tissues from stage 24 embryos using anti-Dg, anti E-cadherin, and anti $\beta_1$-integrin antibodies. No significant decreases of E-cadherin and $\beta_1$ integrin were discerned, while Dg was extinguished in the Mo-injected epidermis. Equal loading is shown by tubulin immunodetection. (N) qRT-PCR from CMo and DgMo tissues performed at stages 15 and 24 and normalized to ornithine decarboxylase expression. Surprisingly, the *E-cadherin* expression is significantly increased in Mo-injected tissues. NS: not significant. Scale bars: 10 μm.

## Dg is a key element of epidermal differentiation

To test whether the abnormal morphology of inner cells in DgMo-injected embryos is associated with a failure of their differentiation, we examined DgMo-injected embryos using a molecular marker, the transcription factor P63, which is expressed during differentiation of the sensorial layer (Lu *et al.*, 2001; Barton *et al.*, 2009). The embryos were unilaterally injected with either the CMo or DgMo. The injected cells were followed using fluorescein isothiocyanate (FITC)-dextran. In CMo embryos observed at stage 24 by indirect immunofluorescence, the sensorial layer of cells was flattened and expressed P63 (Figure 5A). In DgMo epidermis, cells in the deep layer did not express P63, suggesting that they failed to differentiate (Figure 5B). On the other hand, qRT-PCR experiments showed a decrease of *X-p63* expression in DgMo embryos after the neurula stage (Figure 5C). All together, these results suggest that Dg is a key element of epidermal differentiation as it contributes to maintain the expression of the known marker of cell differentiation in the deep layer. They also suggest that the regulation of *X-p63* transcription might be downstream of Dg–ligand interactions.

These results show depletion of Dg affects the interactions between cells and laminin involved in epidermal differentiation. To attempt to confirm and validate these results, overexpression of a mutated Dg missing the intracellular β-C-terminus tail (*Dg-ΔCyto*) was performed. SEM analyses of embryos expressing *Dg-ΔCyto* showed phenotypes partially similar to those of DgMo embryos. As in DgMo, ciliated cells were irregularly scattered and their number at the embryonic surface was reduced (Figure S2, A and C). Similar to DgMo, in situ hybridization for α-tubulin transcripts showed that some of the positive cells were not able to reach the outer layer in the injected side of the embryos, compared with the noninjected one, suggesting that their intercalation was affected (Figure S2B). However, analysis of P63 distribution revealed

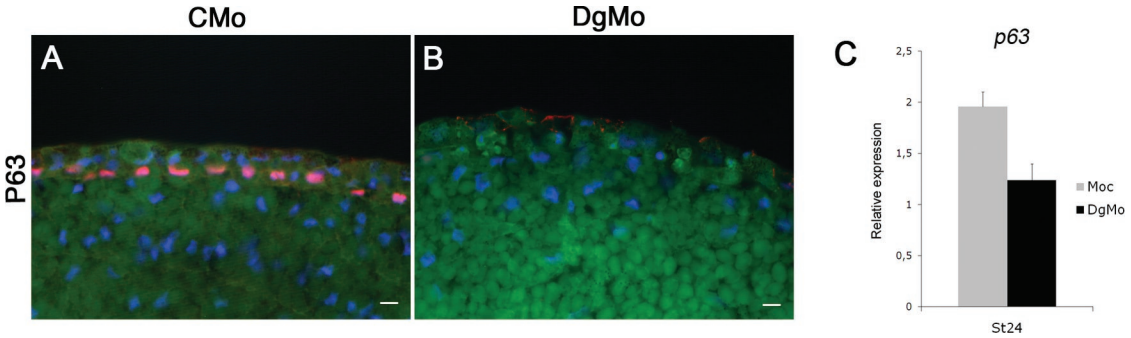


FIGURE 5: P63 expression disappears in Dg-depleted embryos. (A–B) Embryos were unilaterally injected with CMo or DgMo + FITC-dextran as a cell lineage tracer, allowed to develop until stage 24, and then fixed and cryostat-sectioned. An indirect immunofluorescence was performed for P63. Pictures show a merge with dextran (green), P63 (red), and nuclei (blue). In CMo context, a strong labeling of P63 is visible in all nuclei of the inner layer of epidermis (A), while there is a total lack of P63 when embryos are injected with the DgMo (B). (C) qRT-PCR from CMo and DgMo tissues performed at stage 24 and normalized to ornithine decarboxylase expression. The *p63* expression is significantly down-regulated in Mo-injected tissues. Scale bars: 10 μm.

that the protein was expressed in the nuclei (Figure S2D). Concerning the distribution and organization of laminin (Figure S2, E–F), we observed that linear deposition of laminin under the deep layer of epidermal cells was disrupted (compare Figure 7, J and K, later in the article with Figure S2E). Laminin was irregularly deposited at basal poles of cells in the deep layer (Figure S2E, white arrows). Its organization in the matrix was affected, since the fibrils were shortened and, in particular, the network of laminin fibrils appeared discontinuous (Figure S2F).

### Notch signaling pathway regulates *X-dg* transcription in the epidermal ectoderm

Notch is a well-known regulator of lateral inhibition, a contact-mediated signaling whereby a cell that adopts a particular fate inhibits its immediate neighbors from acquiring the same fate. In the epidermal ectoderm, lateral inhibition occurs during gastrulation (Deblandre *et al.*, 1999), before the expression of Dg (Figure 1E). So, inhibiting Notch signaling by expressing a DNA-binding mutant of Su(H) (Su(H)$^{DBM}$) leads to a dramatic increase in the density of the CCPs, while activating Notch signaling by expressing the intracellular domain of Notch (Notch$^{ICD}$) results in a complete loss of α-*tubulin*-expressing cells (Deblandre *et al.*, 1999). Since we never observed overlapping expression of α-*tubulin* and *X-dg* in cells within the inner layer at stage 15, we hypothesized that the Notch pathway might regulate *X-dg* expression. At the four-cell stage, we injected 1) mRNA encoding Su(H)$^{DBM}$ into both left blastomeres or 2) Notch$^{ICD}$ mRNA in one ventral blastomere. In *su(H)$^{DBM}$*-injected embryos observed at stage 19, the α-*tubulin*-expressing cells in the injected side were adjacent and formed several layers in thickness, while the number of *X-dg*–expressing cells in the inner layer of the ectoderm was considerably reduced, compared with the control side (Figure 6, A and C). At stage 24, in the injected side, a large fraction of CCPs remained trapped below the outer layer of the epidermis, the sensorial layer cells did not flatten, and only a few of them expressed *X-dg*; in the more severe cases, there was a total absence of *X-dg* expression (Figure 6D). These results were confirmed by qRT-PCR, which also showed a decrease in the expression of *X-dg* (stages 15–24) following Notch inhibition (Figure 6G). Similar to what was observed in DgMo-treated embryos, indirect immunofluorescence showed an absence of P63 protein expression following Notch inhibition (Figure 6J) and qRT-PCR revealed a decreased expression of *X-p63* mRNAs (Figure 6L). As expected, inhibiting the Notch pathway increased the number of CCPs, but this inhibition also dramatically reduced the number of *X-dg*–expressing cells in the sensorial layer of epidermal ectoderm. Consequently, *p63* was down-regulated. In contrast, the activation of the Notch pathway by *notch$^{ICD}$* corresponded to a total loss of the α-tubulin-positive cells in the inner layer of the epidermis at stage 19, while the number of *X-dg*–expressing cells increased. These cells were adjacent and organized in multiple layers (Figure 6E). At stage 24, in the injected side, the *X-dg* expression increased. *X-dg*–expressing cells were organized in a single layer (Figure 6F) or in several layers of thickness (unpublished data) and had not flattened, probably because the amount of space available became restricted. All the nuclei of the inner cells expressed P63 (Figure 6K). qRT-PCR showed an increase of *X-dg* and *X-p63* mRNAs for each stage from stage 15 to stage 24 (Figure 6, H and M, respectively).

These results demonstrate that inhibition or activation of the Notch pathway prevents or promotes transcription of *X-dg*, respectively, and that Dg is downstream of Notch.

### The rescues of phenotypes reveal an epistatic relationship among Notch, Dg, and P63

The results discussed in the preceding section strongly suggest an epistatic relationship among Notch, Dg, and P63. To confirm this possibility, we attempted to rescue the *su(H)$^{DBM}$* phenotypes by overexpressing *X-dg*. We coinjected *su(H)$^{DBM}$* and the full-length *X-Dg* (*FL-dg*; Moreau *et al.*, 2003) *FL-dg* mRNA in the two left cells of four-cell embryos. The quantification of CCPs using acetylated α-tubulin antibodies showed a twofold increase in the outer layer of the injected side relative to the control (Figure 7, A–E). At stage 24, the shape of cells, the organization of the inner cell layer, and the nuclear expression of P63 were all rescued (see Figure 7, F and H). We also observed that laminin deposition (Figure 7, I–K) and organization (Figure 7L) were restored in the ECM. Thus the concomitant blocking of Notch and overexpression of *X-dg* rescued the intercalation processes with a number of differentiated ciliated cells substantially increased. It rescued the structure of the deep layer, the deposition and organization of laminin, and the expression of P63. To further investigate the cross-talk between Notch and Dg, we tested whether the DgMo phenotypes might be reversed by activation of the Notch pathway. Embryos were coinjected with DgMo and Notch$^{ICD}$ mRNA at the four-cell stage in the left ventral blastomere. We found a loss of the α-tubulin–positive cells in the epidermis, as expected, since the Notch pathway, which is upstream of Dg expression, is activated (Figure 7, M and M′). On the other hand, we showed nuclear expression of P63 protein in the inner epidermal

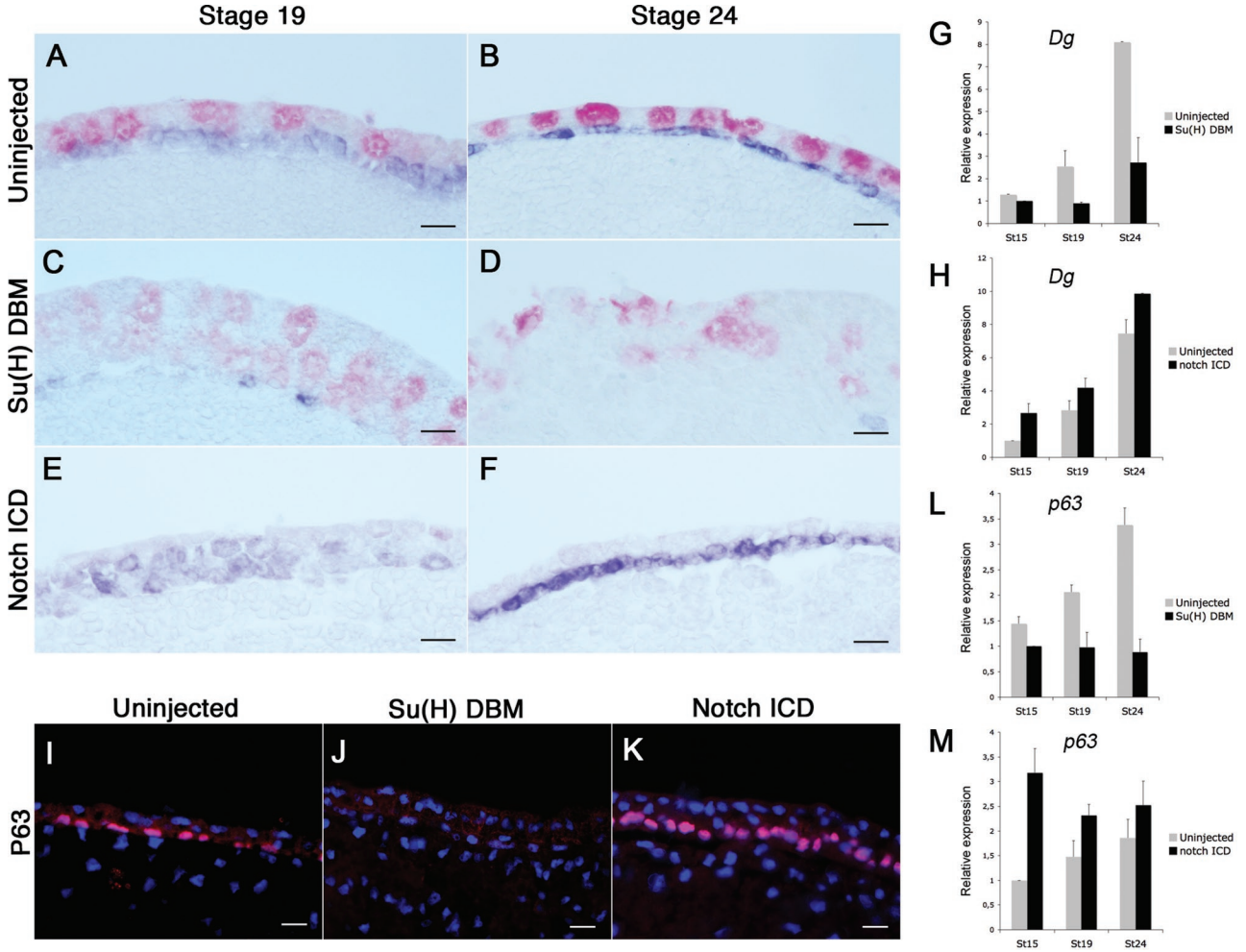


FIGURE 6: Notch signaling controls *X-dg* transcription and consequently *p63* in embryonic epidermal ectoderm. (A–F) Embryos were injected at the four-cell stage in both left blastomeres with *su(H)*$^{DBM}$ or *notch*$^{ICD}$ mRNA and fixed at stages 19 and 24. Embryos were double-labeled by whole-mount, in situ hybridization for *X-dg* (blue purple) and α-*tubulin* (red) and sectioned. At stage 19: labeling shows a normal distribution of CCPs (red) and *X-dg*–expressing cells in the uninjected side (A). Injection of *su(H)*$^{DBM}$ mRNA causes an increase of the number of CCPs, a decrease number of cell expressing *X-dg* transcripts, and a thickening of the skin due to several layers of CCPs (C). Conversely, in the *notch*$^{ICD}$-injected side, there is an absence of CCPs and the number of *X-dg*–expressing cells is increased; these cells are organized in multilayers (E). At stage 24: in the uninjected side, labeling shows a strong expression of α-*tubulin* in the outer layer and of *X-dg* in the inner layer. Cells of the inner layer are cohesive and flat (B). On the *su(H)*$^{DBM}$-injected side, in the most marked phenotype, *X-dg*–positive cells have disappeared and the epidermis is organized in multilayers with numerous α-*tubulin*-positive cells (D). In the *notch*$^{ICD}$-injected side, the α-*tubulin*–positive cells are absent in the outer layer, while the *X-dg*–expressing cells are numerous in the inner layer. These cells are cohesive but have not flattened (F). (I–K) At stage 24, immunostaining was performed for P63. Pictures show a merge of P63 (red) and nuclei (blue). The uninjected side shows a strong labeling of P63 in the inner layer of epidermis (I), while there is a total lack of P63 for embryos injected with the *su(H)*$^{DBM}$ mRNA (J). Conversely, in the *notch*$^{ICD}$-injected side, the number of P63-positive cells is increased in the inner layer (K). (G–M) qRT-PCR from stages 15–24. The expression of *X-Dg* (G) and *p63* (L) are decreased by *su(H)*$^{DBM}$ mRNA injection, while expression of *X-Dg* (H) and *p63* (M) are increased by *notch*$^{ICD}$ mRNA injection (H). Scale bars: 10 μm.

cells of the injected side (Figure 7N). We also showed laminin deposition and its fibrillar organization at the basal pole of inner cells (Figure 7, O and P). This demonstrated that laminin deposition and organization, as well as differentiation of inner cells, were rescued. This rescue may be related to the presence of Dg protein. When Notch$^{ICD}$ was overexpressed, the number of *X-dg*–expressing cells was greater, followed by a titration of DgMo leading to the traduction of Dg protein (Figure S3).

The above results, obtained by inhibition/activation of the Notch pathway, and these rescued phenotypes clearly show that Dg is involved in skin morphogenesis downstream of the Notch signaling pathway. They also show an epistatic relationship among Notch, Dg, and P63 in control of skin morphogenesis.

## DISCUSSION

We observed defects in laminin deposition and organization of the fibronectin network on the basal surface of epidermal ectoderm resulting from Dg depletion. Dg is one of the known laminin receptors. Data in mice (Williamson *et al.*, 1997) and our observations on pronephros development (Bello *et al.*, 2008) and somitogenesis

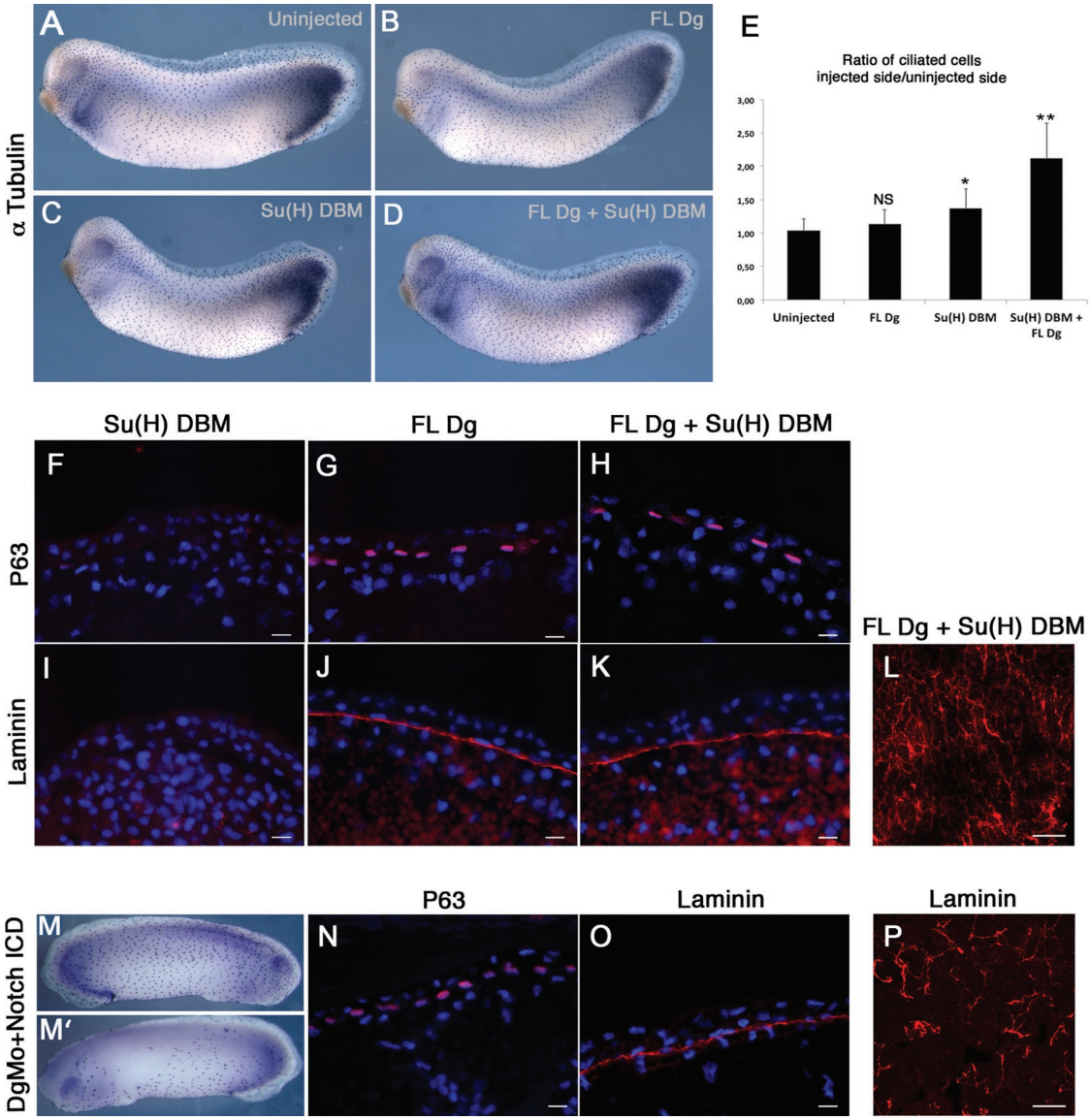


FIGURE 7: Epistatic relationship among Notch, Dg, and p63. (A–D) Embryos were injected with *FL-dg (F), su(H)$^{DBM}$ (G),* or *su(H)$^{DBM}$* + *FL-dg* mRNA (H), then fixed at stage 29/30, and whole-mount immunostaining of α-tubulin with 6-11B-1 antibodies was performed. (E) Ratio analysis of the number of ciliated cells of the injected side/uninjected side shows an increase of 30% of ciliated cells in embryos injected with *su(H)$^{DBM}$* mRNA compared with uninjected embryos, and an increase of 100% in embryos injected with *su(H)$^{DBM}$* + *FL-dg* mRNA. Statistically significant difference (*, *t* test: p = 0.05; **, *t* test: p = 0.01). (F–K) Embryos were coinjected at the four-cell stage in both left blastomeres with *su(H)$^{DBM}$* and *FL-dg* mRNA and fixed at stage 24. Indirect immunofluorescence was performed on cross-sections for P63 (F–H) and laminin (I–K). Expression of P63 and laminin was lost in embryos injected with *su(H)$^{DBM}$* mRNA (F and I), normal in embryos injected with *FL-dg* mRNA (G and J), and rescued in embryos injected with *su(H)$^{DBM}$* + *FL-dg* mRNA (H and K). (L) Whole mount of the basal face of the epidermis from embryos injected with *su(H)$^{DBM}$* + *FL-dg* mRNA (stage 19). The laminin matrix is restored; fibrils are organized in a network. (M–P) Embryos were coinjected at the four-cell stage in the left ventral blastomere with DgMo and Notch$^{ICD}$ mRNA and fixed at stage 24. (M, M′) Whole-mount immunostaining of α-tubulin; (M) noninjected side and (M′) injected side. As expected, there are significantly fewer positive cells in the embryonic site where Notch pathway is activated. (N–O) Indirect immunofluorescence performed on cross-sections for P63 (N) and laminin (O). The expression of both proteins was restored. (P) Whole mount of the basal face of the epidermis from embryos injected with DgMo and Notch$^{ICD}$ mRNAs (stage 19). Laminin was organized in fibrils scattered at the cell surface. NS: not significant. Scale bars: 10 μm.

(Hidalgo *et al.*, 2009) described this critical role of Dg during early development. Recently it has been shown that PAR-1b plays indispensable roles for extracellular laminin assembly through regulation of the localization and function of the Dg complex (Masuda-Hirata *et al.*, 2009). However, it seems Dg may not be required for the appropriate formation of all BMs. Indeed, studies on Dg-null chimeric mice show that Dg is not involved in the formation of skeletal muscle BM (Cote *et al.*, 1999). Moreover, the depletion of Dg using morpholinos indicates Dg is not essential for the assembly of laminin-1 in both inner limiting membrane and Bruch's membrane during *Xenopus laevis* eye development (Lunardi *et al.*, 2006) or in BM of zebrafish embryo (Parsons *et al.*, 2002). Therefore

it is possible that in some tissues other molecules or mechanisms may compensate for the lack of Dg function. For example, one possibility is that integrins contribute to the ECM assembly.

Integrin subunits $\beta_1$, $\alpha_3$, and $\alpha_6$, as well as α-Dg knockouts, all demonstrate the importance of these proteins for the correct assembly of the BMs (Stephens *et al.*, 1995; Henry and Campbell, 1998). Several studies have suggested a functional influence of Dg on integrins. For example, in mouse embryonic stem cells, it has been shown that Dg–laminin interaction is essential for the initial binding of laminin to the cell surface. In contrast, $\beta_1$ integrins were required for subsequent laminin matrix assembly (Henry *et al.*, 2001). We showed that $\beta_1$ integrin subunits are expressed on epidermal ectoderm cells treated with morpholinos, and in spite of this expression, the cells do not accumulate laminin on their surfaces. These findings suggest that Dg and $\beta_1$-integrin functions are nonoverlapping with respect to cell surface laminin-1 binding and assembly.

In addition to the absence of laminin on the basal cell surface, we observed a disorganization of the fibronectin network. In amphibian embryos, fibronectin matrix is assembled on the blastocoel roof during gastrulation. Cytoskeletal tension plays an important role in fibronectin matrix assembly. Dzamba *et al.* (2009) showed that matrix assembly on the blastocoel roof occurs through a cadherin-dependent mechanism. They proposed a new model to explain the regulation of fibronectin assembly in tissues. This model implicates cytoskeleton tension generated by cadherin adhesion complexes. When Dg is depleted, we observed a disorganization of the fibronectin network. This disorganization is observed during neurulation (when Dg begins to be expressed in control embryos). Since $\beta_1$-integrin expression is not affected by Dg depletion, the observed effect on the fibronectin network is likely independent of the binding of fibronectin to $\beta_1$ integrin. We also observed a decrease in E-cadherin expression at the cell–cell contact, which could lead to a decrease of cytoskeleton tension. According to the model of Dzamba *et al.* (2009), the weak cytoskeleton tension will interfere with the organization of the fibronectin network.

Another consequence of Dg depletion concerns CCP intercalation. This key step in skin formation occurs between neurulae stages 16 and 19, just after the beginning of Dg expression. In DgMo-treated embryos, the number of CCPs in the inner layer is identical to that of control embryos. However, the number of CCPs able to insert in the outer layer is reduced. Stubbs *et al.* (2006) observed that when CCPs are overproduced by *su(H)$^{DBM}$* treatment, the ectodermal outer layer imposes spatial limitations in their intercalation processes. In DgMo embryos, the CCP number is unchanged, so we can conclude Dg is also involved in the intercalation process. Furthermore, Dg overexpression rescues CCP intercalation in *su(H)$^{DBM}$* embryos. Differentiated ciliated cells are in this case more numerous than in the control with relation to the increase of CCP number. So, Dg is one key to the regulation of CCP intercalation. Dg can act directly as a component of a signaling cascade or indirectly via its role in laminin ECM deposition. Dg is known to be directly implicated in different signaling pathways (reviewed by Bozzi *et al.*, 2009). Dg may act as a protein scaffold that sequesters these proteins in separate cellular locations to regulate their adhesion-dependent activation (Spence *et al.*, 2004). Members of the laminin glycoprotein family are required for BM assembly and cell polarization, with subsequent effect on cell survival and tissue organization during metazoan embryogenesis (Li *et al.*, 2003). Laminin alone has been shown to promote specific fates in different tissues. Mouse and human neural stem cell precursors differentiate into neurons, astrocytes, and specific glia on laminin, but not on fibronectin (Flanagan *et al.*, 2006). Multipotent embryonic lung cells can be induced to differentiate into smooth muscle cells on laminin (Nguyen and Senior, 2006). Nevertheless, we cannot exclude that other molecules participate in these events, since ECM can bind soluble/secreted factors and maintain them in the extracellular spaces, and thereby function as a repository. The consequence of such interactions may be to restrict or promote access of ligands to cognate cell-surface receptors. It is known that Dg can modulate the cell cycle in human cells by affecting extracellular signal-regulated kinase levels (Higginson *et al.*, 2008). We observed in Dg-depleted embryos a decrease of cell proliferation in accordance with these observations. Other ligands may concern those of the BMP family. In zebrafish DNp63 is a known target of BMP signaling. *p63*, a member of the *p53* gene family, is required for mammalian epidermal development (Levrero *et al.*, 2000; Yang and McKeon, 2000; Irwin and Kaelin, 2001). In DgMo or *su(H)$^{DBM}$* embryos, we observed an absence of P63 in sensorial layer cells, while P63 is expressed in Dg-ΔCyto embryos. These results suggest that the extracellular ligands of the *p63*-activating pathway interact with Dg. Stubbs *et al.* (2006) described Notch suppression of the appearance of not just CCPs but also of INCs, another kind of intercalating cells that move into the outer layer (Drysdale and Elinson, 1992). So, there are two cell populations in the sensorial layer of the epidermis: the first is positively controlled by Notch, express *X-Dg*, and *p63*; the second is negatively controlled by Notch and corresponds to the cells that will intercalate (i.e., CCPs and INCs). In this paper, we demonstrated that, downstream of the Notch signaling pathway, Dg is required for the inner layer differentiation and CCPs intercalation. Further experiments will be necessary to determine if this control is direct or due to the particular cell fate dependent on Notch regulation.

To conclude, these data suggest a cascade of events that induce cell fate in skin progenitors and regulate epidermal differentiation. These events require the correct assembly of the BM for access of different ligands to their receptors. The assembly of the epidermal ECM is directly controlled by Dg. Finally, the data demonstrate an epistatic relationship among Notch, Dg, and P63 to induce cell fate in skin progenitors and control the morphogenesis of the skin (Figure 8). Further elucidation of the transcriptional program controlled by Notch/Dg and identification of modulators of interactions with E-cadherin and laminin will likely provide new insights into the mechanisms underlying morphogenesis, maintenance, and tumorigenesis of the skin.

## MATERIALS AND METHODS

### Embryos, morpholinos, RNA, and injections

*Xenopus laevis* embryos were obtained using standard methods and staged according to Nieuwkoop and Faber (1994). The Dg morpholino antisense oligonucleotide (DgMo) and the mismatch *dg* control morpholino (CMo) were previously described (Bello *et al.*, 2008; Hidalgo *et al.*, 2009). Depending on the experiment, morpholino oligos were injected either in both left blastomeres at the four-cell stage (16 ng per blastomere), or in the four animal blastomeres at the eight-cell stage (8 ng per blastomere). For Western blot analysis, embryos were injected in both blastomeres at the two-cell stage (32 ng of morpholinos). The templates for *notch$^{ICD}$* and *su(H)$^{DBM}$*, full-length *dg* (*FL-dg*), and mutated *dg* missing the β-C-terminus tail (*dg-ΔCyto*) mRNA synthesis have been described (Chitnis *et al.*, 1995; Wettstein *et al.*, 1997; Bello *et al.*, 2008; Hidalgo *et al.*, 2009). mRNA injections were delivered at the four-cell stage into the animal region of the two left blastomeres for *su(H)$^{DBM}$* (1.5 ng per blastomere), *FL-dg* (200 pg per blastomere), and *dg-ΔCyto* (1.3 ng per blastomere) or left ventral

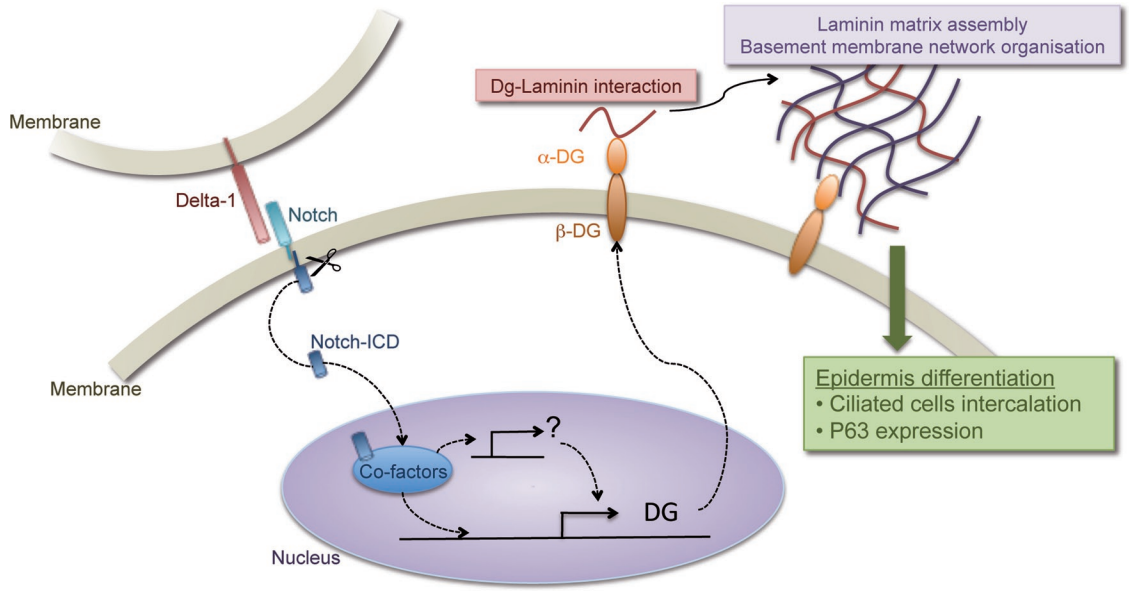


FIGURE 8: Schematic model of Dg function in epidermal ectoderm differentiation. The data established that the Notch signaling pathway activates *X-dg* transcription in inner cell precursors of the epidermal ectoderm. As a result, the inner cell precursors set up the laminin in the ECM, allowing the access of ligands to their receptors. This activates a cascade of events that promotes the intercalation of the precursors of ciliated cells and the expression of P63, which are required for epidermal differentiation.

blastomere for *notch*$^{ICD}$ (1 ng). Membrane-tagged GFP mRNA (GFP-ras mRNA) was injected as cell membrane tracer and FITC-dextran as a cell lineage tracer.

### SEM and thin sections

SEM was carried out as previously described (Steinman, 1968; Billett and Gould, 1971). A Cambridge S-260 scanning electron microscope (Cambridge, UK) was used for observations. Thin sections (0.5 µm) were stained with a toluidine blue solution. Light imaging was done with a Nikon Eclipse 80i (Nikon Instrument, France).

### Hybridization

Whole-mount, in situ hybridization was carried out as described elsewhere (Harland, 1991). The embryos were fixed in MEMFA (0.5 M MOPS, pH 7.4, 100 mM EGTA, 1 mM MgSO4, 3.7% formaldehyde). The antisense or control sense-strand RNA probes from *X-dg* (Moreau *et al.*, 2003) and *α-tubulin* (Deblandre *et al.*, 1999) were generated from linearized plasmids using either digoxigenin (DIG) or fluorescein RNA-labeling mix (Roche, Basel, Switzerland). For double whole-mount, in situ hybridization, the embryos were hybridized with both probes at the same time under standard conditions. After detection of the first probe with the DIG alkaline phosphatase (ALP) antibody (1:2000; Roche) and BCIP/NBT (Sigma-Aldrich, St. Louis, MO), embryos were washed in MeOH 100%; rehydrated in MeOH/MAB (100 mM maleic acid, 150 mM NaCl); and blocked in MAB, 2% Boehringer Mannheim Blocking reagent (Roche), and 20% heat-inactivated sheep serum. Following incubation with fluorescein ALP antibody (1:5000; Roche), the ALP reaction was performed with Fast Red (Sigma).

### Transplants

Surface cell transplants were performed on early-gastrula-stage embryos in Danilchik's medium as described by Drysdale and Elinson (1992). An outer layer of ectoderm from a membrane-tagged GFP mRNA-injected embryo was grafted on the inner layer of a noninjected, CMo- or DgMo-injected embryo. After healing, embryos were transferred to 0.1× MMR medium (Euromedex, Souffelweyersheim, France) with antibiotics. Embryos were allowed to develop until at least stage 28 and fixed in MEMFA. The fluorescent transplant was peeled out from the embryo and treated for immunochemistry.

### Immunochemistry

Embryos fixed in MEMFA were incubated with the mouse monoclonal 6-11B-1 antibodies that recognize acetylated α-tubulin (1:100; Sigma) and with the anti–mouse ALP-conjugated antibody (1:40,000; Jackson Immunoresearch, West Grove, PA). BCIP/NBT was used for the color reaction. Positive cells were counted in both the injected and the uninjected sides using ImageJ software (http://rsb.info.nih.gov/ij/download.html).

Epidermis fragments were peeled on embryos (stage 19 or 24), fixed with MEMFA or 4% PFA on ice (for cadherin and integrin detection), and dehydrated in ethanol. For frozen sections, embryos were embedded in cold-water fish gelatin/sucrose as previously described (Bello *et al.*, 2008). The sections were performed at 14-µm thickness in a cryostat (CM3050 S, Leica). Peeled fragments or sections were blocked in 10% goat serum. The following primary antibodies were used: rabbit anti-GFP (1:500; Abcam, Cambridge, MA), mouse anti–acetylated tubulin 6-11B-1 (1:500; Sigma), mouse anti–ZO-1 (1:50; Invitrogen, Carlsbad, CA), rabbit anti–laminin-1 (1:25; Sigma), mouse anti–fibronectin 4H2 (1:100; D. DeSimone, University of Virginia), mouse anti–$\beta_1$ integrin (1:500; D. Alfandari, University of Massachusetts), anti–E-cadherin 5D3 (1:100; Developmental Studies Hybridoma Bank, University of Iowa, Iowa City, IA), anti-P63 (1:50; Abcam); mouse anti–β-Dg (1:50; A. Menarini Diagnostics, Florence, Italy). After undergoing washing, sections or fragments were incubated with the appropriate secondary antibody: anti–rabbit FITC-conjugated (1:40; Jackson Immunoresearch), anti–rabbit tetramethylrhodamine B isothiocyanate. (1:100; Jackson Immunoresearch), anti–mouse CY3-conjugated (1:100; Sigma), anti–mouse immunoglobin G1 (IgG1) Alexa Fluor 633 (1:1000; Molecular Probes, Invitrogen), anti–mouse IgG2b Alexa Fluor 568 (1:1000; Molecular Probes,

Invitrogen). Nuclear staining was carried out with Hoechst H33258 (1:1000; Sigma).

### qRT-PCR

Total RNAs were isolated from the epidermis of 20 embryos (stage 15, 19, and 24) using the RNeasy mini kit (Qiagen, Valencia, CA) according to the manufacturer's instructions. All primers were designed using Primer Express Software. PCR reactions were carried out using SYBR green (Applied Biosystems, Bedford, MA) on a 7700 Sequence Detector cycler (Applied Biosystems). All experiments were repeated at least three times on separate injections and the qRT-PCR was also performed in triplicate. The results were analyzed using the $2^{-\Delta\Delta Ct}$ method (Livak and Schmittgen, 2001). The relative expression of *X-dg* is shown normalized to the expression of the housekeeping gene *ODC*. The qRT-PCR *X-dg*, *X-p63*, and *E-cadherin* primers are as follows:

| | |
|---|---|
| *X-dg* sense: | TCCCCACAGAATTTCTCGCT |
| Antisense: | GTAACCAAGAGGGCAATGTCTCC |
| *p63* sense: | AGCAAAGTCAGCCACCTGGA |
| Antisense: | GTTTTGGCAATCTGACAGTAGAGC |
| *E-cadherin* sense: | CGTGTGGCTTTGCGGACT |
| Antisense: | CTGCATTTATGGAAGGCACAAC |

### Western blots

Morpholinos were injected in both cells at the two-cell stage. At stage 24, embryos were homogenized in lysis buffer (1% Triton X100, 150 mM NaCl, pH 7.5, 10 mM Tris, 1 mM EDTA, 1 mM ethyleneglycoltetraacetic acid [EGTA], 0.5% NP-40, 0.2 mM phenylmethyl sulfonyl fluoride [PMSF]) supplemented with protease inhibitors. Samples were separated by 10% SDS–PAGE and transferred to nitrocellulose membrane (Hybond, GE Healthcare, Waukesha, WI). The membrane was incubated with the following primary antibodies: mouse anti–β Dg 43DAG1/8D5 (1:25; Abcam), mouse anti–E-Cadherin 5D3 (1:500; Developmental Studies Hybridoma Bank), mouse anti–$\beta_1$ integrin (1:500; D. Alfandari). It was then incubated with anti–mouse antibody coupled to peroxidase (1:10,000; Jackson Immunoresearch). Identification was made by chemiluminescence (SuperSignal West Pico Chemiluminescent substrate kit, Pierce, Thermo Scientific, Lafayette, CO). The membrane was then dehybrided and incubated with mouse anti–α-tubulin antibody DM1A (1:10,000; Sigma) and with anti–mouse antibody conjugated with peroxidase (1:10,000; Jackson Immunoresearch). Identification was made by chemiluminescence as previously. For quantification, blots were exposed on x-ray films for various time points, and the films were scanned and analyzed using ImageJ software.

### Proliferation assays

Proliferation assays were performed in whole embryos (n = 20), fixed in MEMFA at stage 24, and then stained with the rabbit anti–human phosphohistone H3 antibody (1:100; Ser 10, mitosis marker, Euromedex, Souffelweyersheim, France) and the anti–rabbit ALP-conjugated (1:5000; Jackson Immunoresearch). Positive cells were counted in both the injected and the uninjected sides using ImageJ software.

### Membrane fluorescence intensity quantification

After acquisition, images were imported into ImageJ software for analysis. Mean pixel intensity of a fixed area of the cell membrane was quantified and corrected by the subtraction of the mean pixel intensity of an area of the same size from the cytoplasm. Twenty measurements were taken from each group, and all experiments were repeated at least three times on separate injections. Results are expressed as the ratio of the average of the mean intensity ± SE.

## ACKNOWLEDGMENTS

We thank Dominique Alfandari for $\beta_1$-integrin antibody, Kris Kintner for α-*tubulin*, Thomas Pieler and Anne-Hélène Monsoro-Burq for *notch*$^{ICD}$, Muriel Umbauher for GFP and *su(H)*$^{DBM}$, Douglas W. DeSimone for fibronectin antibodies, and Dominique Alfandari and Clémence Carron for critical reading of the manuscript. We also thank Richard Schwartzmann for confocal microscopy, Isabelle Le Disquet for SEM, Cyrielle Sophie for thin sections, Sophie Gournet for schematic drawings, and Noémie Reigner for providing help with the language.

## REFERENCES

Bakkers J, Hild M, Kramer C, Furutani-Seiki M, Hammerschmidt M (2002). Zebrafish DeltaNp63 is a direct target of Bmp signaling and encodes a transcriptional repressor blocking neural specification in the ventral ectoderm. Dev Cell 2, 617–627.

Barresi R, Campbell KP (2006). Dystroglycan: from biosynthesis to pathogenesis of human disease. J Cell Sci 119, 199–207.

Barton CE, Tahinci E, Barbieri CE, Johnson KN, Hanson AJ, Jernigan KK, Chen TW, Lee E, Pietenpol JA (2009). DeltaNp63 antagonizes p53 to regulate mesoderm induction in *Xenopus laevis*. Dev Biol 329, 130–139.

Bateman JF, Boot-Handford RP, Lamande SR (2009). Genetic diseases of connective tissues: cellular and extracellular effects of ECM mutations. Nat Rev Genet 10, 173–183.

Bello V, Sirour C, Moreau N, Denker E, Darribere T (2008). A function for dystroglycan in pronephros development in *Xenopus laevis*. Dev Biol 317, 106–120.

Billett FS, Gould RP (1971). Fine structural changes in the differentiating epidermis of *Xenopus laevis* embryos. J Anat 108, 465–480.

Bozzi M, Morlacchi S, Bigotti MG, Sciandra F, Brancaccio A (2009). Functional diversity of dystroglycan. Matrix Biol 28, 179–187.

Chitnis A, Henrique D, Lewis J, Ish-Horowicz D, Kintner C (1995). Primary neurogenesis in *Xenopus* embryos regulated by a homologue of the *Drosophila* neurogenic gene *Delta*. Nature 375, 761–766.

Cote PD, Moukhles H, Lindenbaum M, Carbonetto S (1999). Chimaeric mice deficient in dystroglycans develop muscular dystrophy and have disrupted myoneural synapses. Nat Genet 23, 338–342.

Deblandre GA, Wettstein DA, Koyano-Nakagawa N, Kintner C (1999). A two-step mechanism generates the spacing pattern of the ciliated cells in the skin of Xenopus embryos. Development 126, 4715–4728.

Drysdale TA, Elinson RP (1992). Cell migration and induction in the development of the surface ectodermal pattern of the *Xenopus laevis* tadpole. Dev Growth Differ 34, 51–59.

Durbeej M, Larsson E, Ibraghimov-Beskrovnaya O, Roberds SL, Campbell KP, Ekblom P (1995). Non-muscle alpha-dystroglycan is involved in epithelial development. J Cell Biol 130, 79–91.

Dzamba BJ, Jakab KR, Marsden M, Schwartz MA, DeSimone DW (2009). Cadherin adhesion, tissue tension, and noncanonical Wnt signaling regulate fibronectin matrix organization. Dev Cell 16, 421–432.

Ervasti JM, Campbell KP (1991). Membrane organization of the dystrophin-glycoprotein complex. Cell 66, 1121–1131.

Fey J, Hausen P (1990). Appearance and distribution of laminin during development of *Xenopus laevis*. Differentiation 42, 144–152.

Flanagan LA, Rebaza LM, Derzic S, Schwartz PH, Monuki ES (2006). Regulation of human neural precursor cells by laminin and integrins. J Neurosci Res 83, 845–856.

Harland RM (1991). *In situ* hybridization: an improved whole-mount method for *Xenopus* embryos. Methods Cell Biol 36, 685–695.

Henry MD, Campbell KP (1998). A role for dystroglycan in basement membrane assembly. Cell 95, 859–870.

Henry MD, Satz JS, Brakebusch C, Costell M, Gustafsson E, Fassler R, Campbell KP (2001). Distinct roles for dystroglycan, β1 integrin and perlecan in cell surface laminin organization. J Cell Sci 114, 1137–1144.

Hidalgo M, Sirour C, Bello V, Moreau N, Beaudry M, Darribere T (2009). In vivo analyzes of dystroglycan function during somitogenesis in *Xenopus laevis*. Dev Dyn 238, 1332–1345.

Higginson JR, Thompson O, Winder SJ (2008). Targeting of dystroglycan to the cleavage furrow and midbody in cytokinesis. Int J Biochem Cell Biol 40, 892–900.
Irwin MS, Kaelin WG (2001). p53 family update: p73 and p63 develop their own identities. Cell Growth Differ 12, 337–349.
Keller RE (1980). The cellular basis of epiboly: an SEM study of deep-cell rearrangement during gastrulation in *Xenopus laevis*. J Embryol Exp Morphol 60, 201–234.
Levrero M, De Laurenzi V, Costanzo A, Gong J, Wang JY, Melino G (2000). The p53/p63/p73 family of transcription factors: overlapping and distinct functions. J Cell Sci 113, 1661–1670.
Li S, Edgar D, Fassler R, Wadsworth W, Yurchenco PD (2003). The role of laminin in embryonic cell polarization and tissue organization. Dev Cell 4, 613–624.
Livak KJ, Schmittgen TD (2001). Analysis of relative gene expression data using real-time quantitative PCR and the 2(-Delta Delta C(T)) Method. Methods 25, 402–408.
Lu P, Barad M, Vize PD (2001). *Xenopus* p63 expression in early ectoderm and neurectoderm. Mech Dev 102, 275–278.
Lunardi A, Cremisi F, Dente L (2006). Dystroglycan is required for proper retinal layering. Dev Biol 290, 411–420.
Lunardi A, Dente L (2002). Molecular cloning and expression analysis of dystroglycan during *Xenopus laevis* embryogenesis. Mech Dev 119 (suppl 1), S49–S54.
Masuda-Hirata M, Suzuki A, Amano Y, Yamashita K, Ide M, Yamanaka T, Sakai M, Imamura M, Ohno S (2009). Intracellular polarity protein PAR-1 regulates extracellular laminin assembly by regulating the dystroglycan complex. Genes Cells 14, 835–850.
Michele DE *et al*. (2002). Post-translational disruption of dystroglycan-ligand interactions in congenital muscular dystrophies. Nature 418, 417–422.
Mills AA, Zheng B, Wang XJ, Vogel H, Roop DR, Bradley A (1999). p63 is a p53 homologue required for limb and epidermal morphogenesis. Nature 398, 708–713.
Moreau N, Alfandari D, Gaultier A, Cousin H, Darribere T (2003). Cloning and expression patterns of dystroglycan during the early development of *Xenopus laevis*. Dev Genes Evol 213, 355–359.
Nguyen NM, Senior RM (2006). Laminin isoforms and lung development: all isoforms are not equal. Dev Biol 294, 271–279.
Nieuwkoop PD, Faber J (1994). Normal Table of *Xenopus laevis*, New York: Garland Publishing.
Nokhbatolfoghahai M, Downie JR, Clelland AK, Rennison K (2005). The surface ciliation of anuran amphibian embryos and early larvae: patterns, timing differences and functions. J Nat Hist 39, 887–929.
Parsons MJ, Campos I, Hirst EM, Stemple DL (2002). Removal of dystroglycan causes severe muscular dystrophy in zebrafish embryos. Development 129, 3505–3512.
Spence HJ, Dhillon AS, James M, Winder SJ (2004). Dystroglycan, a scaffold for the ERK-MAP kinase cascade. EMBO Rep 5, 484–489.
Steinman RM (1968). An electron microscopic study of ciliogenesis in developing epidermis and trachea in the embryo of *Xenopus laevis*. Am J Anat 122, 19–55.
Stephens LE, Sutherland AE, Klimanskaya IV, Andrieux A, Meneses J, Pedersen RA, Damsky CH (1995). Deletion of beta 1 integrins in mice results in inner cell mass failure and peri-implantation lethality. Genes Dev 9, 1883–1895.
Stubbs JL, Davidson L, Keller R, Kintner C (2006). Radial intercalation of ciliated cells during *Xenopus* skin development. Development 133, 2507–2515.
Tsang KY, Cheung MC, Chan D, Cheah KS (2010). The developmental roles of the extracellular matrix: beyond structure to regulation. Cell Tissue Res 339, 93–110.
Van Agtmael T, Bruckner-Tuderman L (2010). Basement membranes and human disease. Cell Tissue Res 339, 167–188.
Weir ML, Oppizzi ML, Henry MD, Onishi A, Campbell KP, Bissell MJ, Muschler JL (2006). Dystroglycan loss disrupts polarity and beta-casein induction in mammary epithelial cells by perturbing laminin anchoring. J Cell Sci 119, 4047–4058.
Wettstein DA, Turner DL, Kintner C (1997). The *Xenopus* homolog of *Drosophila Suppressor of Hairless* mediates Notch signaling during primary neurogenesis. Development 124, 693–702.
Williamson RA, Henry MD, Daniels KJ, Hrstka RF, Lee JC, Sunada Y, Ibraghimov-Beskrovnaya O, Campbell KP (1997). Dystroglycan is essential for early embryonic development: disruption of Reichert's membrane in Dag1-null mice. Hum Mol Genet 6, 831–841.
Wilson PA, Hemmati-Brivanlou A (1995). Induction of epidermis and inhibition of neural fate by Bmp-4. Nature 376, 331–333.
Winder SJ (1997). The membrane-cytoskeleton interface: the role of dystrophin and utrophin. J Muscle Res Cell Motil 18, 617–629.
Yang A, McKeon F (2000). P63 and P73: P53 mimics, menaces and more. Nat Rev Mol Cell Biol 1, 199–207.
Yang A *et al*. (1999). p63 is essential for regenerative proliferation in limb, craniofacial and epithelial development. Nature 398, 714–718.